



**HAL**  
open science

## On the actual anode area that contributes to the current density produced by electroactive biofilms

Alessandro Carmona Martinez, Rémy Lacroix, Eric Trably, Serge da Silva,  
Nicolas Bernet

### ► To cite this version:

Alessandro Carmona Martinez, Rémy Lacroix, Eric Trably, Serge da Silva, Nicolas Bernet. On the actual anode area that contributes to the current density produced by electroactive biofilms. *Electrochimica Acta*, 2018, 259, pp.395-401. 10.1016/j.electacta.2017.10.200 . hal-02626318

**HAL Id: hal-02626318**

**<https://hal.inrae.fr/hal-02626318>**

Submitted on 26 May 2020

**HAL** is a multi-disciplinary open access archive for the deposit and dissemination of scientific research documents, whether they are published or not. The documents may come from teaching and research institutions in France or abroad, or from public or private research centers.

L'archive ouverte pluridisciplinaire **HAL**, est destinée au dépôt et à la diffusion de documents scientifiques de niveau recherche, publiés ou non, émanant des établissements d'enseignement et de recherche français ou étrangers, des laboratoires publics ou privés.

# Accepted Manuscript

On the actual anode area that contributes to the current density produced by electroactive biofilms

Alessandro A. Carmona-Martínez, Rémy Lacroix, Eric Trably, Serge Da Silva, Nicolas Bernet



PII: S0013-4686(17)32346-0

DOI: [10.1016/j.electacta.2017.10.200](https://doi.org/10.1016/j.electacta.2017.10.200)

Reference: EA 30586

To appear in: *Electrochimica Acta*

Received Date: 11 August 2017

Revised Date: 18 October 2017

Accepted Date: 31 October 2017

Please cite this article as: A.A. Carmona-Martínez, Ré. Lacroix, E. Trably, S. Da Silva, N. Bernet, On the actual anode area that contributes to the current density produced by electroactive biofilms, *Electrochimica Acta* (2017), doi: 10.1016/j.electacta.2017.10.200.

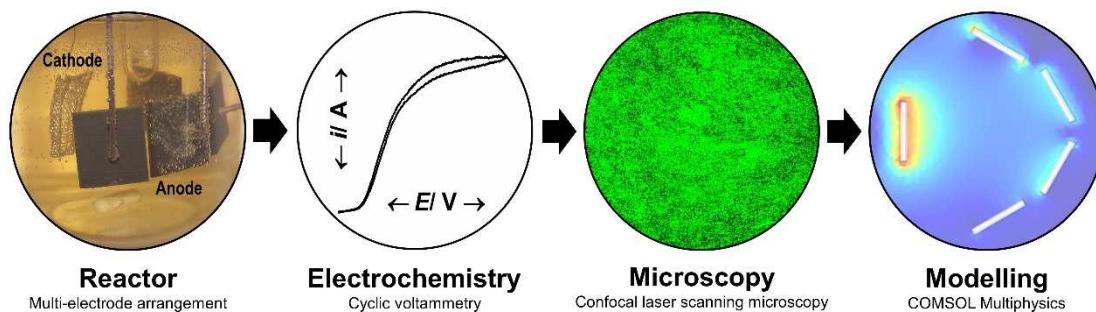
This is a PDF file of an unedited manuscript that has been accepted for publication. As a service to our customers we are providing this early version of the manuscript. The manuscript will undergo copyediting, typesetting, and review of the resulting proof before it is published in its final form. Please note that during the production process errors may be discovered which could affect the content, and all legal disclaimers that apply to the journal pertain.

Comment citer ce document :

Carmona Martinez, A., Lacroix, R., Trably, E., Da Silva, S., Bernet, N. (Auteur de correspondance) (2018). On the actual anode area that contributes to the current density produced by electroactive biofilms. *Electrochimica Acta*, 259, 395-401. , DOI : 10.1016/j.electacta.2017.10.200

## Graphical abstract

On the consensus of the anode area that contributes to microbial current via:



Comment citer ce document :

Carmona Martinez, A., Lacroix, R., Trably, E., Da Silva, S., Bernet, N. (Auteur de correspondance) (2018). On the actual anode area that contributes to the current density produced by electroactive biofilms. *Electrochimica Acta*, 259, 395-401. , DOI : 10.1016/j.electacta.2017.10.200

# 1 On the actual anode area that contributes to the current density 2 produced by electroactive biofilms

3 Alessandro A. Carmona-Martínez<sup>a,c</sup>, Rémy Lacroix<sup>b</sup>, Eric Trably<sup>a</sup>, Serge Da Silva<sup>b</sup> and Nicolas Bernet<sup>a,\*</sup>

4 <sup>a</sup>LBE, INRA, 102, Avenue des Etangs, Narbonne, 11100, France

5 <sup>b</sup>GT-MIC Ingénieries, ZI de VIC les Graves, 9, Rue du Développement, 31 320 Castanet Tolosan, France

6 <sup>c</sup>Present adress: IMDEA Water Institute, Technological Park of the University of Alcalá, Alcalá de Henares, Spain

7 \*Corresponding author: N. Bernet, LBE, INRA, 102 Avenue des Etangs, Narbonne, 11100, France, E-mail:  
8 nicolas.bernet@inra.fr; T: +33 (0)4 68 42 51 74

## 10 Abstract

11 Even with an increasing interest in scaling-up Microbial Electrochemical Technologies  
12 (MET), it is still common to focus on their “fundamentals”. An important example is the  
13 production of current density ( $j_{max}$ ) by microbial anodes in a three-electrode arrangement  
14 (3EA) configuration, e.g.: a graphite plate of well-defined projected (or geometric) surface  
15 area (PSA) and a cathode, both parallel to each other.

16 With such type of anode within a 3EA configuration,  $j_{max}$ 's calculation is expected to be  
17 straightforward. Nonetheless, certain issues prevail. Occasionally,  $j_{max}$  is wrongly  
18 overestimated neglecting the surface of the anode that does not directly face the cathode.

19 Here, grown biofilms of the novel electroactive bacterium *Geoalkalibacter subterraneus*  
20 showed that the actual area of anode that contributes to  $j_{max}$  is the total PSA (or apparent  
21 geometric area) immersed in the electrolyte available to form a biofilm regardless the side of  
22 the anode that faced or opposed the cathode even in a medium with low conductivity such as  
23 urban wastewater, a niche of application for METs.

24 For the sake of normalization, researchers (and especially a “freshman” microbial  
25 electrochemist) are encouraged to: A) use the total PSA (or apparent geometric area)  
26 immersed in the electrolyte to calculate  $j_{max}$  or B) to cover edges and faces hidden of the  
27 anode with an electrical insulator to allow the flow of current on the side of the anode that  
28 directly faces the cathode prior calculation of  $j_{max}$ . This normalization can be conducted when  
29 the main goal is to quantify (and thus properly report)  $j_{max}$  produced when using (e.g.): a novel  
30 i) electroactive bacterium, ii) electrode material or iii) reactor design.

31 **Keywords:** *Electroactive biofilm • Geoalkalibacter subterraneus • COMSOL Multiphysics® •*  
32 *Electrode surface area • Microbial electrochemical technologies • Current density*

## 33 1. Introduction

34 Microbial Electrochemical Technologies (METs) take advantage of the electron transfer (ET)  
35 interactions occurring between electroactive bacteria (EAB) and electrode materials [1]. The  
36 use of these interactions impacts several rapid evolving technological fields ranging from the  
37 treatment of wastewater by the integration of METs into conventional treatment technologies  
38 [2], via the desalination of brackish water in microbial desalination cells [3], to the production  
39 of value-added molecules such as acetate from CO<sub>2</sub> via microbial electrosynthesis [4].

40 Although several parameters are used to evaluate the performance of METs, such as the  
41 product yield or the coulombic efficiency, the calculation of the maximum current density  
42 ( $j_{max}$ ) per projected (or apparent geometric) surface area (PSA) of anode material is among  
43 one of the most widely accepted parameters [5]. Despite the efforts to standardize the  
44 calculation of  $j_{max}$  to use the reported value for comparison among different studies, certain  
45 issues prevail regarding its proper calculation.

46 In three-electrode arrangement (3EA) experimental set-ups where a two-side planar anode  
47 (hereafter WE from “working electrode”) is used in parallel to a cathode (henceforth CE from  
48 “counter electrode”),  $j_{max}$  is occasionally calculated neglecting the surface of the WE that does  
49 not directly face the CE [6]. This causes  $j_{max}$  to be wrongly overestimated, which in turn  
50 prohibits an objective comparison of results among studies.

51 When considering for example the case of a WE with dimensions of 2.5 x 2.5 x 0.25 cm,  
52 some might use only the side of the WE that faces the CE to calculate  $j_{max}$  (i.e.: 6.25 cm<sup>2</sup>).  
53 However, in multiple experiments it is usually observed that the biofilm grows on all the  
54 immersed anode material which is in contact with the electrolyte (i.e. both electrode sides plus  
55 edges: 15.00 cm<sup>2</sup>, see Fig. A7 in Appendix A). Depending on the methodology used to  
56 calculate the surface area,  $j_{max}$  can therefore vary by a factor of 2.4.

57 This overestimation might be due to the direct extrapolation of the information extracted from  
58 strictly electrochemical electrode processes’ books. Such information is usually employed for  
59 the interpretation of microbial electron transfer mechanisms between electrodes and EAB that  
60 might be governed by completely different phenomena. As an example of this, it is reported in  
61 text books of fundamental electrochemistry that  $j_{max}$  strongly depends on the WE’s proximity  
62 to the CE [7]. Thus, it is usually assumed that the current produced on the side of the WE that  
63 directly faces the CE will be significantly higher than the current produced on the back side of  
64 the WE that does not directly faces the CE [8] (please see Fig. A1 in Appendix A).

65 This manuscript proposes a consensus on the actual total PSA of anode that contributes to  
66  $j_{max}$ . Experiments were carried out with biofilms of the novel EAB *Geoalkalibacter*  
67 *subterraneus* and subjected to a multi-approach analysis with techniques that span from  
68 electrochemistry via microscopy to modelling. This is not an attempt to evaluate the overall  
69 performance of a bioelectrochemical device by its produced anodic current density alone as  
70 would be typical for MFC research.

71

## 72 2. Experimental

### 73 2.1. Overall experimental strategy

74 A three-electrode arrangement was used (Fig. 1A). Four graphite plate anodes (WE) faced a  
75 single platinum-iridium cathode (CE). In the middle of the reactor a SCE reference electrode  
76 (RE) was placed. While WE1, WE2 and WE3 were chronoamperometrically (CA) and  
77 individually controlled at +200 mV vs. SCE, WE4 was not. A N-Stat (N) configuration was  
78 used, as similarly described by [9]. The N-Stat configuration allowed each WE to be  
79 connected to a separate potentiostat channel sharing the same RE and CE according to  
80 BioLogic's connection mode protocol. In the N-Stat configuration, the multi-channel  
81 potentiostat individually controls each anode with respect to a single RE.

82 On all WEs the growth of pure culture anodic biofilms of the novel EAB *Geoalkalibacter*  
83 *subterraneus* (henceforth *Glk. subterraneus* [10]) was followed by Confocal laser scanning  
84 microscopy (CLSM). Biofilm growth on anodes was allowed (green "tick" symbol in Fig. 1A)  
85 or limited by an electrical insulator (red "cross" symbol in Fig. 1A).

86 -Please insert **Figure 1** here-

### 87 2.2. Maintenance and growth of *Geoalkalibacter subterraneus*

88 The growth and maintenance of *Glk. subterraneus* was carried out exactly as previously  
89 detailed elsewhere [10]. *Glk. subterraneus* was chosen here as a model EAB due to its shared  
90 similar electrochemical characteristics with the extensively well characterized EAB *Geobacter*  
91 *sulfurreducens* in terms of its  $j_{max}$  and its electron transfer mechanism [11].

92 All chemicals were of analytical or biochemical grade and were purchased from Sigma-  
93 Aldrich and Merck. All media preparations were adjusted to pH 7, vigorously flushed with N<sub>2</sub>  
94 gas (purity  $\geq$  99.9999, Linde France S.A.) for at least 30 min using a commercial air stone (or  
95 aquarium bubbler) and then autoclaved (121°C for 20 min).

96 Sterile growth medium FRR was used for routinely culture maintenance and contained (per  
97 L): 17.0 g of NaCl, 4.50 g of MgCl<sub>2</sub>·6H<sub>2</sub>O, 0.35 g of CaCl<sub>2</sub>·2H<sub>2</sub>O, 1.00 g of NH<sub>4</sub>Cl, 0.08 g  
98 KH<sub>2</sub>PO<sub>4</sub>, 3.50 g of NaHCO<sub>3</sub>, 3.00 g of Yeast extract, 1 mL of trace element solution, 1 mL of  
99 selenite-tungstate solution and 1.00 g of CH<sub>3</sub>COONa as electron donor.

### 100 2.3. Electrode preparation and Bioelectrochemical set-up

101 Preparation of electrodes and bioelectrochemical reactors was exactly conducted in agreement  
102 to a procedure reported elsewhere [10]. In brief: working electrodes were 2.5 cm x 2.5 cm x  
103 0.25 cm planar graphite plates (C000440/15, Goodfellow SARL, 229 Rue Solférino, F-59000  
104 Lille, France) screwed onto 2 mm diameter, 15 cm long titanium rods (TI007910/13,  
105 Goodfellow) that ensured electrical connection. Planar graphite electrodes were used as  
106 delivered by the provider. Counter electrodes were 90% Platinum-10% Iridium grids joint by  
107 heating in a blue flame with a 0.5 mm diameter, 15 cm long 90% Platinum-10% Iridium rod  
108 (Heraeus PSP S.A.S., Contact Materials Division, 526, Route des Gorges du Sierroz, 73100  
109 Grésy-sur-Aix France). If not stated otherwise, all potentials provided in this manuscript refer

110 to the Saturated Calomel reference Electrode (SCE) (KCl 3.0 M, +240 mV vs. SHE, Materials  
111 Mates, La Guilletière 38700 Sarcenas, France).

112 To determine the contribution on  $j_{max}$  by both sides of a planar WE as part of the  
113 electrochemical set-up, four WEs were placed in the same electrochemical reactor facing a  
114 CE (Fig. 1A). However, not all the surface of the WE was available for the EAB to form a  
115 biofilm. To accomplish this, one side of the WE material was electrically insulated with a  
116 commercial seal (Siljoint, Bardahl®) to make the covered WE's surface inaccessible for the  
117 EAB. Furthermore, to assure comparability and reproducibility all four WEs were  
118 simultaneously measured in one electrochemical reactor.

#### 119 2.4. Current density ( $j$ ) calculation

120 Current is calculated throughout this manuscript as i) per projected surface area ( $j_{PSA}$ ), which  
121 takes into account the absolute current ( $i_{absolute}$ ) divided by the projected surface area (PSA),  
122 an adequate calculation for compact and smooth electrodes with low degree of surface  
123 imperfections, such as the planar graphite plate electrodes used here, since they have a very  
124 well defined geometric surface area [12]. The mathematical modelling was conducted taking  
125 into account  $j_{PSA}$ . Maximum current density ( $j_{max}$ ) refers to the maximum value extracted from  
126 the Chronoamperometric curve only.

127 Additionally, for sake of completeness current is also reported in Fig. 2 as ii) absolute current  
128 ( $i_{absolute}$ ), which is the current without taking into account the available surface area of anodic  
129 electrode material; and iii) current density as per electrochemically active surface area ( $j_{EASA}$ ),  
130 that is based on the obtained charge by acetate oxidation during Chronoamperometry (i.e.,  
131 integrated current over time). In an attempt to normalize the current to the real surface area of  
132 electrode available for the EAB to form a biofilm the electrochemically active surface area  
133 (EASA) was calculated as previously reported from the Anson equation [12]:

$$134 \quad Q_d = 2 n F EASA C D^{1/2} \pi^{1/2} t^{1/2} \quad (\text{Equation 1})$$

135 Where  $Q_d$  is the charge (C), i.e., current integrated over time from the Chronoamperometric  
136 curve;  $n$  the number of electrons transferred (8 mol  $e^-$ /mol acetate);  $F$  is the Faraday constant  
137 (96485 C/ mol  $e^-$ );  $EASA$  is the electrochemically active surface area ( $\text{cm}^2$ );  $C$  is the  
138 concentration of the substrate ( $1 \times 10^{-5}$  mol acetate/ml);  $D$  the diffusion coefficient of the  
139 substrate ( $1.21 \times 10^{-5}$   $\text{cm}^2/\text{s}$ ); and  $t$  is time (s).  $EASA$  was later used to calculate the current  
140 density with respect to the electrochemically active surface area and plotted in Figure 2C. The  
141 Excel tool used for the calculation of  $EASA$  is provided as supplementary information in  
142 Appendix B.

#### 143 2.5. Cyclic voltammetry data and its processing

144 Cyclic voltammetry (CV) of *Glk. subterraneus* biofilms was carried out under  
145 bioelectrocatalytic substrate consumption (the so-called "turnover conditions").  
146 Chronoamperometric (CA) maximum current densities ( $j_{max}$ ) of established microbial biofilms  
147 were calculated considering the total PSA immersed in the electrolyte and due to the presence  
148 of visible apparent reddish biofilms that covered all the electrode. Here all data are based on

149 experiments of at least two independent biofilm replicates [5] and standard deviations are  
150 presented throughout the manuscript.

## 151 **2.6. Confocal laser scanning microscopy (CLSM) to measure biofilm electrode coverage** 152 **and thickness**

153 *Glk. subterraneus* biofilms grown on WEs were examined by CLSM after staining with  
154 nucleic acid-specific fluorochromes exactly as reported elsewhere [10]. Whole electrodes  
155 were stained using the LIVE/ DEADs BacLight<sup>®</sup> Bacterial Viability Kit (Invitrogen) and  
156 confocal images of electroactive biofilms were acquired with a confocal laser scanning  
157 system (Leica TCS SP2, Leica Microsystems, Wetzlar, Germany).

## 158 **2.7. Modelling of the current density distribution on the electrode surface with** 159 **COMSOL Multiphysics<sup>®</sup>**

160 This type of exemplary modelling approach is more frequently employed to the study of  
161 strictly chemical electrode processes and very rarely employed for the study of the  
162 interactions of EAB embed within biofilms and electrode materials in METs [13-15].  
163 Notwithstanding, the current density produced at each potentiostatically controlled electrode  
164 was later modeled with the software COMSOL Multiphysics<sup>®</sup> in an attempt to graphically  
165 illustrate the total PSA contribution on the current density production in METs.

166 To conduct the modelling, in COMSOL Multiphysics<sup>®</sup> the following parameters were  
167 introduced: A) Reactor geometry; B) Calculated conductivity for the electrolyte used; C)  
168 Polynomial equations for the anodic kinetic reactions; and D) Polynomial equations for the  
169 cathodic kinetic reactions.

170 It is worth noticing that the experiments carried out were originally focused on the anode  
171 performance. The potential of the electrode against the counter electrode has therefore not  
172 been measured during chronoamperometry and cyclic voltammetry. The value of the cell  
173 voltage used in modelling was thus adjusted to 1.1 V to reproduce the results experimentally  
174 observed.

### 175 **2.7.1. Reactor geometry definition in COMSOL Multiphysics<sup>®</sup>**

176 A cylindrical electrochemical reactor as the one shown in Fig. A2 and Fig. A3 was used in the  
177 experiments and its dimensions were used in COMSOL Multiphysics<sup>®</sup>. Its diameter was 10  
178 cm with a height of 6 cm (working volume of 500 ml, i.e.: filled with microbiological medium  
179 for bacteriological growth). As depicted in Section 2.3, four graphite plates were used as  
180 working electrodes. The reference electrode was placed right in the center of the reactor at a  
181 height that did not interfere with the distribution of current and potential. The relative position  
182 of all electrodes is depicted in Fig. 1, A3 and A4 (see Appendix B).

### 183 **2.7.2. Microbiological medium conductivity**

184 With the microbiological medium described in Section 2.2 and the information presented in  
185 Table 1 a conductivity of 5.0 S/m at 25°C was calculated. This value has been introduced into  
186 COMSOL Multiphysics<sup>®</sup> and a simulation has been accordingly conducted. Additionally, a

197 simulation at a conductivity value much lower of 0.1 S/m was conducted since this  
 198 conductivity value is the one usually ascribed to domestic wastewater. At his point, it is good  
 199 to keep in mind that the current applications of METs are thought to be focused on the  
 200 treatment of domestic wastewater.

191 **Table 1. Electrolyte conductivity calculation of the growth medium used in this study.**

Compound "i"	[i] / g L <sup>-1</sup>	[i] / mmol L <sup>-1</sup>	[Cation] / mmol L <sup>-1</sup>	[Anion] / mmol L <sup>-1</sup>	$\lambda_+$ / 10 <sup>-4</sup> m <sup>2</sup> S mol <sup>-1</sup>	$\lambda_-$ / 10 <sup>-4</sup> m <sup>2</sup> S mol <sup>-1</sup>	Conductivity / S m <sup>-1</sup>
NaCl	17.0	290.9	[Na <sup>+</sup> ] = 290.9	[Cl <sup>-</sup> ] = 290.9	Na <sup>+</sup> : 50.1	Cl <sup>-</sup> : 76.3	3.7
MgCl <sub>2</sub> ·6 H <sub>2</sub> O	4.5	22.2	[Mg <sup>2+</sup> ] = 22.2	[Cl <sup>-</sup> ] = 44.4	½ Mg <sup>2+</sup> : 53.0	Cl <sup>-</sup> : 76.3	0.6
NH <sub>4</sub> Cl	1.0	18.7	[NH <sub>4</sub> <sup>+</sup> ] = 18.7	[Cl <sup>-</sup> ] = 18.7	NH <sub>4</sub> <sup>+</sup> : 73.5	Cl <sup>-</sup> : 76.3	0.3
NaHCO <sub>3</sub>	3.5	41.7	[Na <sup>+</sup> ] = 41.7	[HCO <sub>3</sub> <sup>-</sup> ] = 41.7	Na <sup>+</sup> : 50.1	HCO <sub>3</sub> <sup>-</sup> : 44.5	0.4
CH <sub>3</sub> COONa	1.0	12.2	[Na <sup>+</sup> ] = 12.2	[CH <sub>3</sub> COO <sup>-</sup> ] = 12.2	Na <sup>+</sup> : 50.1	CH <sub>3</sub> COO <sup>-</sup> : 41.0	0.1
<b>Total*</b>							<b>5.0</b>

192 Note:  $\lambda_+$  stands for molar cation conductivity at 25°C;  $\lambda_-$  stands for molar anion conductivity at 25°C; \*Total growth medium conductivity  
 193 due to "i" compounds. Due to the high content of NaCl used in this medium preparation, it is evident that the conductivity of the medium it is  
 194 independent of the rest of the additional compounds within the medium and mainly attributed to the NaCl content.

### 195 2.7.3. Anodic reactions' kinetics

196 Anodic kinetic curves were obtained during cyclic voltammetry (CV) under catalytic  
 197 conditions (Fig. A5). Both forward and backward sigmodal-like signals were very similar.  
 198 Thus, only the backward signal was adjusted to a polynomial fitting. CV shown that the three  
 199 electrodes share similar kinetics. Independently of the orientation of the available electrode  
 200 surface the current density obtained by each electrode was very similar as well (see Fig. 3A).

### 201 2.7.4. Cathodic reaction's kinetics

202 The kinetics of the electrolysis of water for hydrogen production at a scan rate of 1 mV/s on a  
 203 Pt/Ir counter electrode was experimentally measured in similar three-electrode arrangement  
 204 set-up as the one previously described, i.e.: graphite working electrode, Pt/Ir counter electrode  
 205 and SCE reference electrode. The medium composition shown in Table 1 was used as  
 206 electrolyte.

## 207 3. Results and Discussion

### 208 3.1. Chronoamperometric current density of *Glk. subterraneus* biofilms

209 In Fig.2 current is shown as i) per projected surface area ( $j_{PSA}$ ), an adequate calculation for  
 210 planar graphite plate electrodes with a very well defined geometric surface area. For sake of  
 211 completeness current is also shown as ii) absolute current ( $i_{absolute}$ ), i.e., the current without  
 212 taking into account the available surface; and iii) current density as per electrochemically  
 213 active surface area ( $j_{EASA}$ ), based on the obtained charge by acetate oxidation during  
 214 Chronoamperometry.

215 After inoculation with cells of *Glk. subterraneus*, the biofilm growth began and it was  
216 illustrated as an exponential-like current production trend as previously described for this  
217 particular EAB [10] (Fig. 2). Interestingly, the biofilm growth was very similar on all WEs as  
218 indicated by the chronoamperometric current production trend. No effect was observed in  
219 terms of current production among WE1, WE2 and WE3. The current density  $j_{max}$  was very  
220 closely similar for WE1, WE2 and WE3, with  $2.60 \pm 0.01$ ,  $2.66 \pm 0.07$  and  $2.57 \pm 0.07$  A/m<sup>2</sup>,  
221 respectively. Although  $j_{max}$  of WE2 was slightly higher with respect to WE1 and WE3, there  
222 was no significant difference between these three WEs.

223 During chronoamperometric measurements the actual area of anode that contributed to  $j_{max}$   
224 was the total PSA (or apparent geometric area) immersed in the electrolyte regardless the side  
225 of the anode that faced the cathode.

### 226 3.1.1. Accurate calculation of current density regarding the porosity of the material

227 As described in the Experimental section, current density was calculated by two methods. The  
228 first one divides the absolute current ( $i_{absolute}$ ) by the geometric projected surface area ( $j_{PSA}$ ).  
229 The second one is an attempt to normalize the current to the real electrochemically active  
230 surface area of electrode available for the EAB to form a biofilm ( $j_{EASA}$ ). In this work, graphite  
231 plate electrodes with a very well defined surface area were used. Nevertheless, when  
232 calculating  $j_{EASA}$  by the method suggested elsewhere it was observed, as expected, that the  
233 available electrochemically active surface area (EASA) was higher than the one geometrically  
234 calculated. Thus,  $j_{EASA}$  was lower than  $j_{PSA}$  since the Anson equation (see equation 1)  
235 somehow provides an approximation of the real EASA available for the EAB to form a  
236 biofilm. It is worth noticing that EASA will always be higher than the geometric surface area  
237 consider in the calculation of  $j_{PSA}$  due to the inherent complex distribution of the EASA at a  
238 microscopic level.

239 -Please insert **Figure 2** here-

### 240 3.2. Direct electron transfer mechanism (ETM)

241 Cyclic voltammetry (CV) is one of the most employed electrochemical techniques in METs to  
242 study at some extent how EAB interact with the electrode material, either anodes or cathodes  
243 [16]. CV is used to decipher the electron transfer mechanism (ETM) by which electrons are  
244 transferred between EAB and electrodes [17]. Here, turnover CV (*i.e.*, under  
245 bioelectrocatalytic substrate consumption conditions) was applied to analyse whether there  
246 was any difference in the ETM of microbial biofilms developed on different sides of the  
247 anode in METs.

248 Independent biofilms grown on WE1, WE2 and WE3 showed an indistinguishable sigmoidal  
249 shape from each other (Fig. 3A). Such shape is typical of EAB able to produce high currents  
250 and thick biofilms via a direct ETM [10]. The similarities in the ETM showed by all anodes  
251 imply that irrespective of the anode side available for biofilm growth, the same ETM is used  
252 at both sides of an anode that faces or opposes a cathode. In Fig. 3A a flat voltammogram  
253 indicates a typical control CV with no electroactive biofilm to illustrate that the sigmoidal CV  
254 shape is caused by the biofilm under catalytic “turnover conditions”.

255 When determining the formal potential ( $E_f$ ) of the ETM by calculating the first derivative of  
256 CVs (Fig. 3B), the  $E_f$  observed for all tested WEs was  $-474.99 \pm 1.29$  mV vs. SCE. Such low  
257 standard deviation confirmed that the EAB within biofilms used the same ETM. This is easily  
258 understood when taking into account that the same scan rate and the same biological  
259 conditions were assured for all WEs since all anodes were hosted within the same  
260 electrochemical reactor.

261 Cyclic voltammetric measurements thus confirm that the actual area of anode that contributed  
262 to the ETM was the total PSA (or apparent geometric area) immersed in the electrolyte  
263 regardless the anode side that faced the cathode.

264 -Please insert **Figure 3** here-

### 265 **3.3. Homogeneous biofilm formation independently of the anode side orientation**

266 Together with the analysis of  $j_{max}$  and ETM on WE1, WE2 and WE3, a microscopic analysis  
267 with CLSM was performed on all anodes (including WE4) to determine any possible effect on  
268 biofilm formation and thickness due to the orientation of the anode.

269 Once again, no appreciable effect was observed whatever the orientation of the anode side  
270 with respect to the cathode. Biofilms on WE1, WE2 and WE3 were similarly covering the  
271 entire apparent available anode PSA (Fig. 4). With the LIVE/DEAD<sup>®</sup> kit, it was possible to  
272 see that WE1, WE2 and WE3 were homogeneously covered by metabolically active cells of  
273 *Glk. subterraneus* with similar thickness values of  $75 \pm 7$ ,  $66 \pm 26$  and  $71 \pm 12$   $\mu\text{m}$ , for WE1,  
274 WE2 and WE3, respectively. CLSM analysis of biofilms not only confirmed a very uniform  
275 coverage of anodes at the microscopic level but also at the macroscopic perspective as  
276 previously observed by visual inspection of a reddish biofilm (see Fig. A2 in Appendix A).

277 WE4 was not potentiostatically controlled. Consistently, no significant biofilm formation was  
278 observed when using CLSM. The thickness value estimated for WE4 ( $13 \pm 1$   $\mu\text{m}$ ) suggests  
279 that the “few” bacterial cells observed by CLSM on the anode surface corresponded to an  
280 heterogeneous deposition of bacterial cells likely detached from the other potentiostatically  
281 controlled anodes (WE1, WE2 and WE3) on which *Glk. subterraneus* successfully formed an  
282 electroactive biofilm.

283 CLSM certified that the actual area of anode that was available for biofilm formation was the  
284 total PSA (or apparent geometric area) immersed in the electrolyte regardless the side of the  
285 anode that faced the cathode.

286 -Please insert **Figure 4** here-

### 287 **3.4. Modelling of the current density distribution on anodes with COMSOL** 288 **Multiphysics<sup>®</sup>**

289 The current density produced at each potentiostatically controlled anode was later modeled  
290 with the software COMSOL Multiphysics<sup>®</sup> in an attempt to graphically illustrate the anode  
291 area contribution on the current density produced in METs (Fig. 5). It was clear that the  
292 anodic current densities are very similar on the available surface areas of each electrode  
293 independently whether the available surface of the anode faced or opposed the cathode.

294 A common argument regarding the calculation of the current density per available surface  
295 area in METs is that at such high conductivity of 5.0 S/m as the one used here all the available  
296 anode surface area will very likely contribute to the current density regardless the side of the  
297 anode that faced the cathode (see Table 1). Thus, a further simulation was conducted at the  
298 typical conductivity found in urban wastewater (0.1 S/m).

299 It was observed that at 0.1 S/m, a decrease of the current density of about 16% can occur on  
300 all WEs when compared to the modelling at 5.0 S/m (data not shown). Nonetheless, the  
301 current density of WE1, WE2 and WE3 is still independent of the orientation of the electrode  
302 surface with respect to the CE.

303 The conducted modelling approach with COMSOL Multiphysics<sup>®</sup> showed that the actual area  
304 of anode that contributes to  $j_{max}$  is the total PSA (or apparent geometric area) immersed in the  
305 electrolyte independently of the side of the anode that faces the cathode even in a medium  
306 with low conductivity such as urban wastewater, a common niche of application for METs.

307 -Please insert **Figure 5** here-

#### 308 **4. Conclusions**

309 The use of a combined approach of electrochemistry, microscopy and modelling for the  
310 analysis of electroactive biofilms formed by *Glk. subterraneus* allowed to determine the  
311 contribution of each anode side orientation on the current density produced in METs. The use  
312 of chronoamperometry showed that no effect was observed whatever the anode orientation  
313 (WE1, WE2 and WE3), since  $j_{max}$  was similar for all anodes potentiostatically controlled.  
314 Turnover cyclic voltammetry of anodes also indicated a common direct electron transfer  
315 mechanism that was confirmed after calculation of their shared formal potential from first  
316 derivative curves. The analysis of biofilms by confocal laser scanning microscopy showed,  
317 once again, no appreciable effect of the anode orientation side with respect to the cathode.  
318 Biofilms on WE1, WE2 and WE3 anodes covered the entire apparent available projected  
319 surface area with clearly similar thickness values ranging from 66 to 75  $\mu\text{m}$ . A modelling  
320 approach supported the experimental observations by confirming that the current densities  
321 were very similar whatever the available anode side considered, *i.e.* anode side that faced or  
322 opposed the cathode. In conclusion and with a purpose of standardization of  $j_{max}$  assessment,  
323 certain areas of the anode (hidden edges or faces) with uncertain electrochemical activity  
324 should be covered with an electrical insulator to further consider only the flow of current on  
325 the side of the anode directly facing the cathode when for example the main goal of the study  
326 is to quantify the current density produced by a novel i) electroactive bacterium, ii) electrode  
327 material or iii) reactor design.

#### 328 **5. Acknowledgements**

329 This research was financed by the French National Research Agency (ANR-09-BioE-10  
330 DéfiH12). A.A.C.M gratefully acknowledges C. Pouzet at the Plateforme d'imagerie FR-AIB,  
331 TRI-Genotoul for technical assistance with CLSM.

#### 332 **6. References**

- 333 [1] S. Patil, C. Hägerhäll, L. Gorton, Electron transfer mechanisms between microorganisms and  
334 electrodes in bioelectrochemical systems, *Bioanalytical Reviews*, 4 (2012) 159-192.
- 335 [2] A. Aguirre-Sierra, T. Bacchetti-De Gregoris, A. Berna, J.J. Salas, C. Aragon, A. Esteve-Nunez,  
336 Microbial electrochemical systems outperform fixed-bed biofilters in cleaning up urban wastewater,  
337 *Environmental Science: Water Research & Technology*, 2 (2016) 984-993.
- 338 [3] Z. Borjas, A. Esteve-Núñez, J.M. Ortiz, Strategies for merging microbial fuel cell technologies in  
339 water desalination processes: Start-up protocol and desalination efficiency assessment, *Journal of*  
340 *Power Sources*, (2017).
- 341 [4] C.W. Marshall, E.V. LaBelle, H.D. May, Production of fuels and chemicals from waste by  
342 microbiomes, *Current Opinion in Biotechnology*, 24 (2013) 391-397.
- 343 [5] B.E. Logan, Essential Data and Techniques for Conducting Microbial Fuel Cell and other Types of  
344 Bioelectrochemical System Experiments, *ChemSusChem*, 5 (2012) 988-994.
- 345 [6] C. Dumas, R.g. Basseguy, A. Bergel, DSA to grow electrochemically active biofilms of *Geobacter*  
346 *sulfurreducens*, *Electrochimica Acta*, 53 (2008) 3200-3209.
- 347 [7] A.J. Bard, L.R. Faulkner, *Electrochemical Instrumentation, Electrochemical Methods:*  
348 *Fundamentals and Applications*, Wiley2000.
- 349 [8] D. Pletcher, *Experimental electrochemistry, A First Course in Electrode Processes*, Royal Society  
350 of Chemistry2009.
- 351 [9] C.I. Torres, R. Krajmalnik-Brown, P. Parameswaran, A.K. Marcus, G. Wanger, Y.A. Gorby, B.E.  
352 Rittmann, Selecting anode-respiring bacteria based on anode potential: Phylogenetic,  
353 electrochemical, and microscopic characterization, *Environmental Science and Technology*, 43 (2009)  
354 9519-9524.
- 355 [10] A.A. Carmona-Martínez, M. Pierra, E. Trably, N. Bernet, High current density via direct electron  
356 transfer by the halophilic anode respiring bacterium *Geoalkalibacter subterraneus*, *Physical*  
357 *Chemistry Chemical Physics*, 15 (2013) 19699-19707.
- 358 [11] N.S. Malvankar, D.R. Lovley, Microbial nanowires for bioenergy applications, *Current Opinion in*  
359 *Biotechnology*, 27 (2014) 88-95.
- 360 [12] M. Sharma, S. Bajracharya, S. Gildemyn, S.A. Patil, Y. Alvarez-Gallego, D. Pant, K. Rabaey, X.  
361 Dominguez-Benetton, A critical revisit of the key parameters used to describe microbial  
362 electrochemical systems, *Electrochimica Acta*, (2014).
- 363 [13] C. Picioreanu, M.C.M. van Loosdrecht, T.P. Curtis, K. Scott, Model based evaluation of the effect  
364 of pH and electrode geometry on microbial fuel cell performance, *Bioelectrochemistry*, 78 (2010) 8-  
365 24.
- 366 [14] E. Dalak, *Evaluation of Unified Numerical and Experimental Methods for Improving Microbial*  
367 *Electrochemical Technologies (MXCs)*, University of Toulouse III - Paul Sabatier, Toulouse, 2012, pp.  
368 91.
- 369 [15] R. Lacroix, S.D. Silva, M.V. Gaig, R. Rousseau, M.-L. Delia, A. Bergel, Modelling potential/current  
370 distribution in microbial electrochemical systems shows how the optimal bioanode architecture  
371 depends on electrolyte conductivity, *Physical Chemistry Chemical Physics*, 16 (2014) 22892-22902.
- 372 [16] F. Harnisch, S. Freguia, A Basic Tutorial on Cyclic Voltammetry for the Investigation of  
373 Electroactive Microbial Biofilms, *Chemistry – An Asian Journal*, 7 (2012) 466-475.
- 374 [17] C.I. Torres, A.K. Marcus, H.S. Lee, P. Parameswaran, R. Krajmalnik-Brown, B.E. Rittmann, A  
375 kinetic perspective on extracellular electron transfer by anode-respiring bacteria, *FEMS Microbiology*  
376 *Reviews*, 34 (2010) 3-17.

377

378

379 **Figure captions:**

380 **Figure 1. (A) Photograph and (B) Top view of the electrode arrangement within the**  
381 **electrochemical reactor showing the relative orientation of the four anodes (WE1-4).** The  
382 availability or electrical insulation of the anode surface is indicated by the green “tick” or red  
383 “cross” symbol, respectively. Anode WE4 was not potentiostatically controlled.

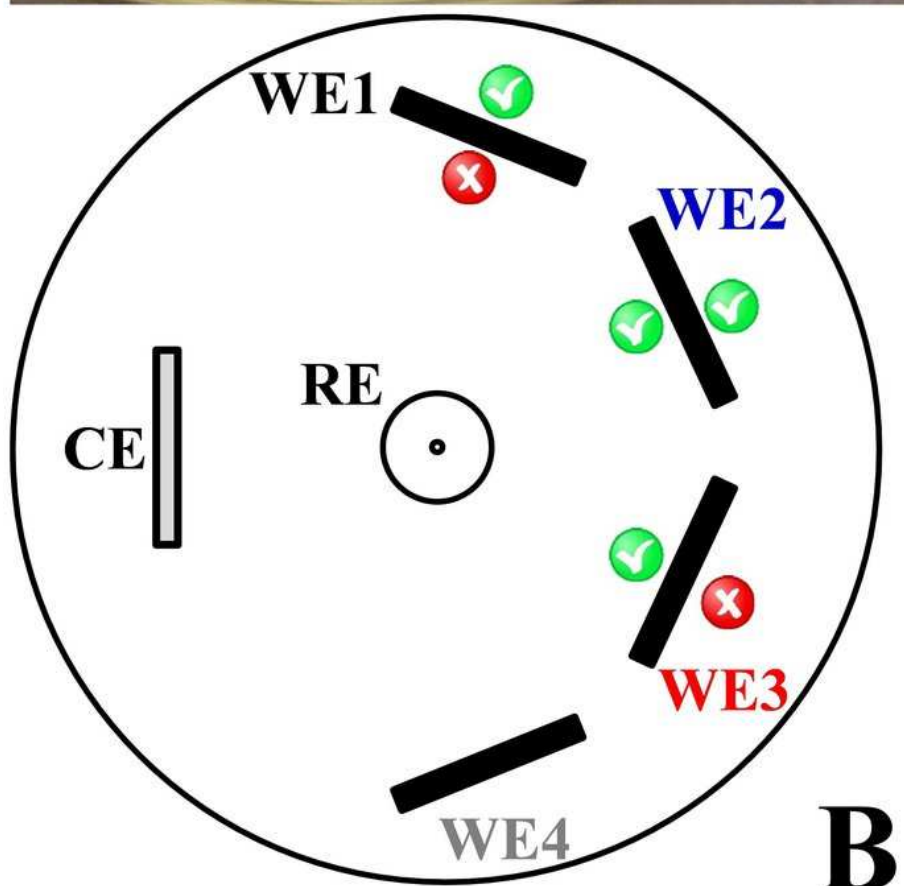
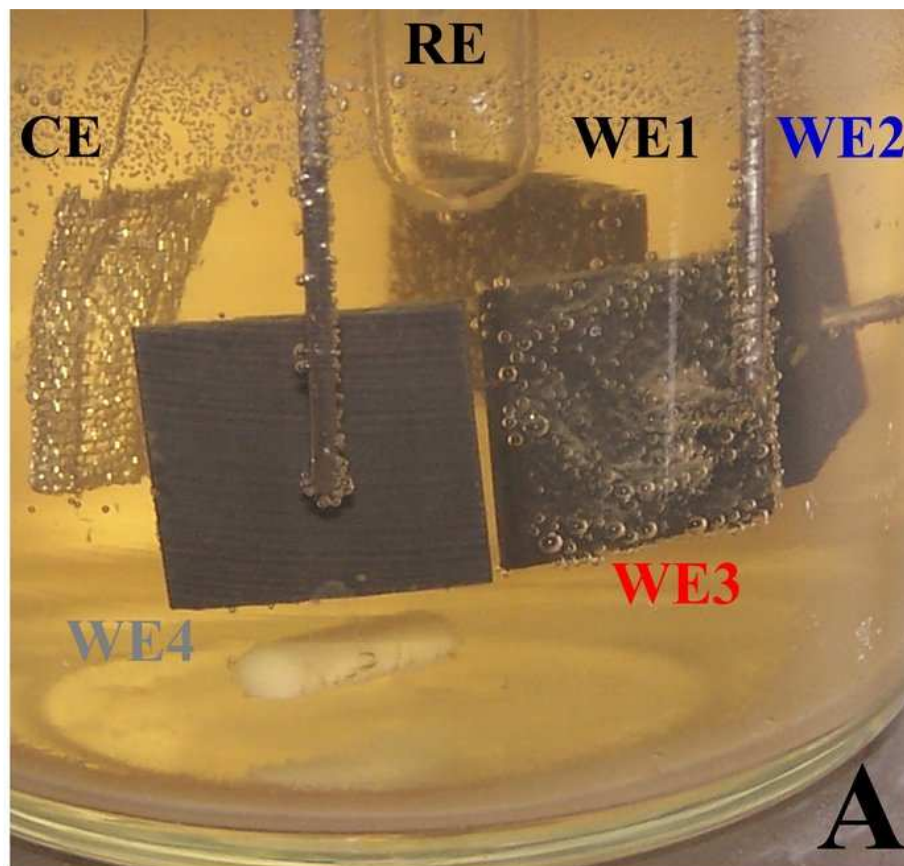
384 **Figure 2. Chronoamperometric current production by biofilms grown on WE1, WE2**  
385 **and WE3 anodes.** A) Absolute current without dividing by the available surface area, B)  
386 Current density by geometric surface and C) Current density calculated by the real  
387 electrochemically active surface area. Thick and thin lines indicate duplicates of the same  
388 experimental condition conducted independently in chronological order. ↓CV: control cyclic  
389 voltammetry (CV) without biofilm; t-CV↑: turnover-CV of biofilm under catalytically active  
390 acetate conversion; CLSM: stop of experiment and biofilm preparation for CLSM analysis.  
391 WE4 was not potentiostatically controlled. Thus, it is not depicted.

392 **Figure 3. A) Turnover cyclic voltammetry (i.e.: under catalytically active acetate**  
393 **conversion) of mature biofilms grown on anodes WE1 (black), WE2 (blue) and WE3**  
394 **(red) and B) their respective first derivative curve.** In A: flat CV indicates control CV  
395 without biofilm. WE4 was not potentiostatically controlled. Thus, it is not depicted.

396 **Figure 4. CLSM maximum intensity projections of mature biofilms on anodes.** It is  
397 shown that independently of the anode side available for biofilm formation its surface is  
398 uniformly covered by *Glk. subterraneus* cells. A projection of WE4 is shown to exemplify  
399 that no significant bacterial cell deposition occurred due to the non “potentiostatically-  
400 controlled” condition of this anode.

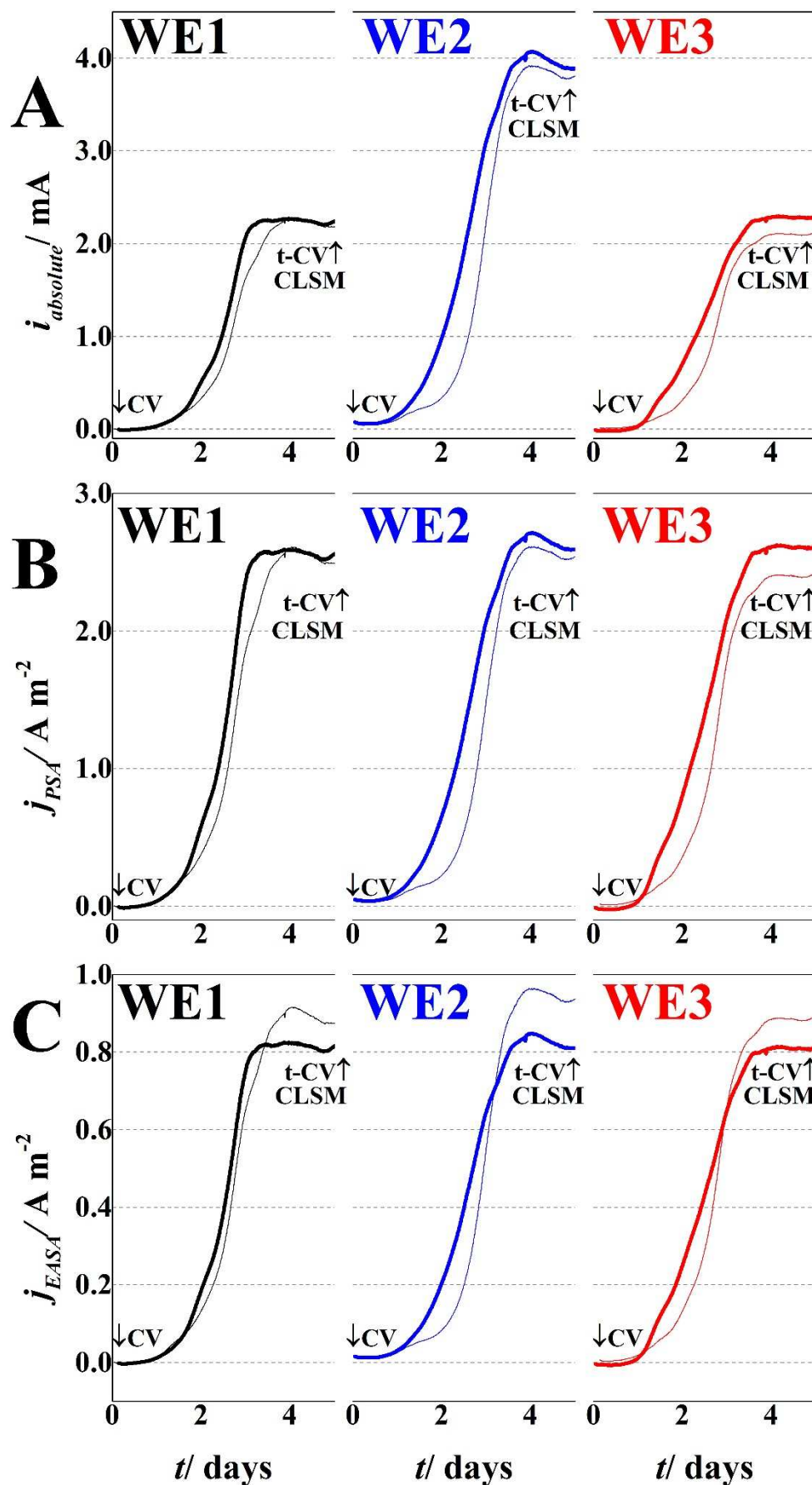
401 **Figure 5. Modelling with COMSOL Multiphysics® of current density distribution on**  
402 **anodes.**

403

404 **Figures:**405 **Figure 1:**

406

407 Figure 2:

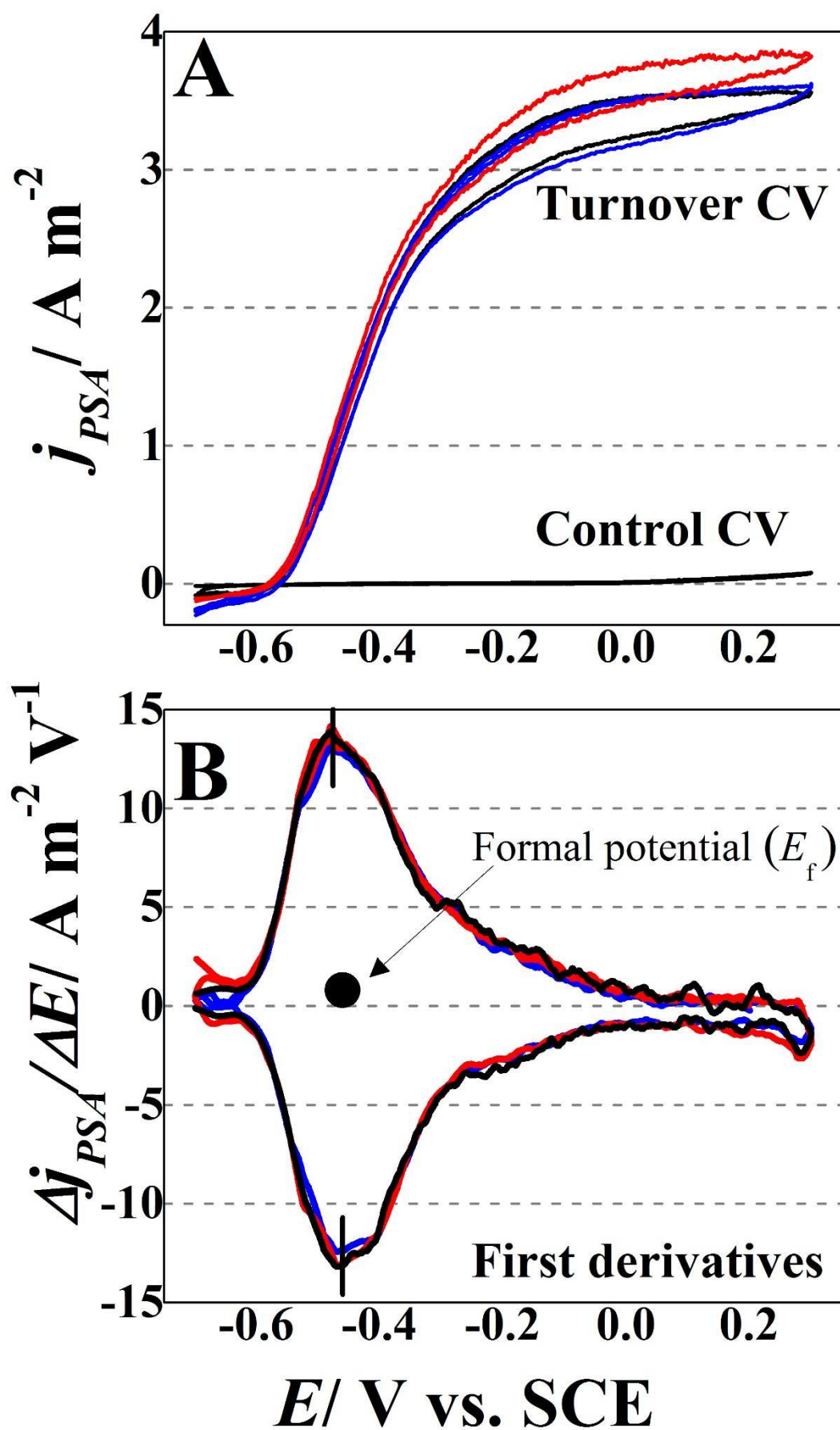


408

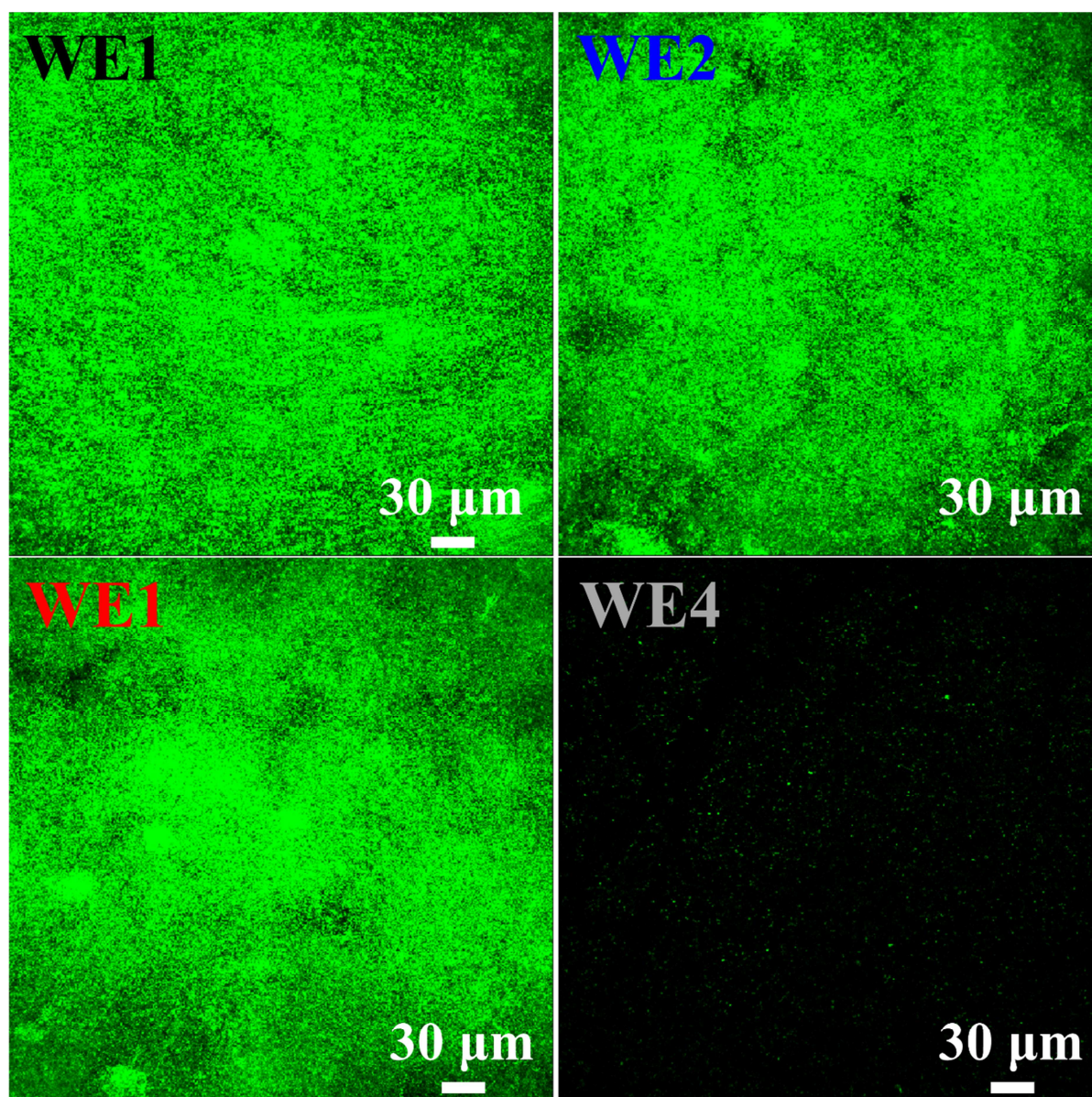
Comment citer ce document :

Carmona Martinez, A., Lacroix, R., Trably, E., Da Silva, S., Bernet, N. (Auteur de correspondance) (2018). On the actual anode area that contributes to the current density produced by electroactive biofilms. *Electrochimica Acta*, 259, 395-401. , DOI : 10.1016/j.electacta.2017.10.200

409 Figure 3:

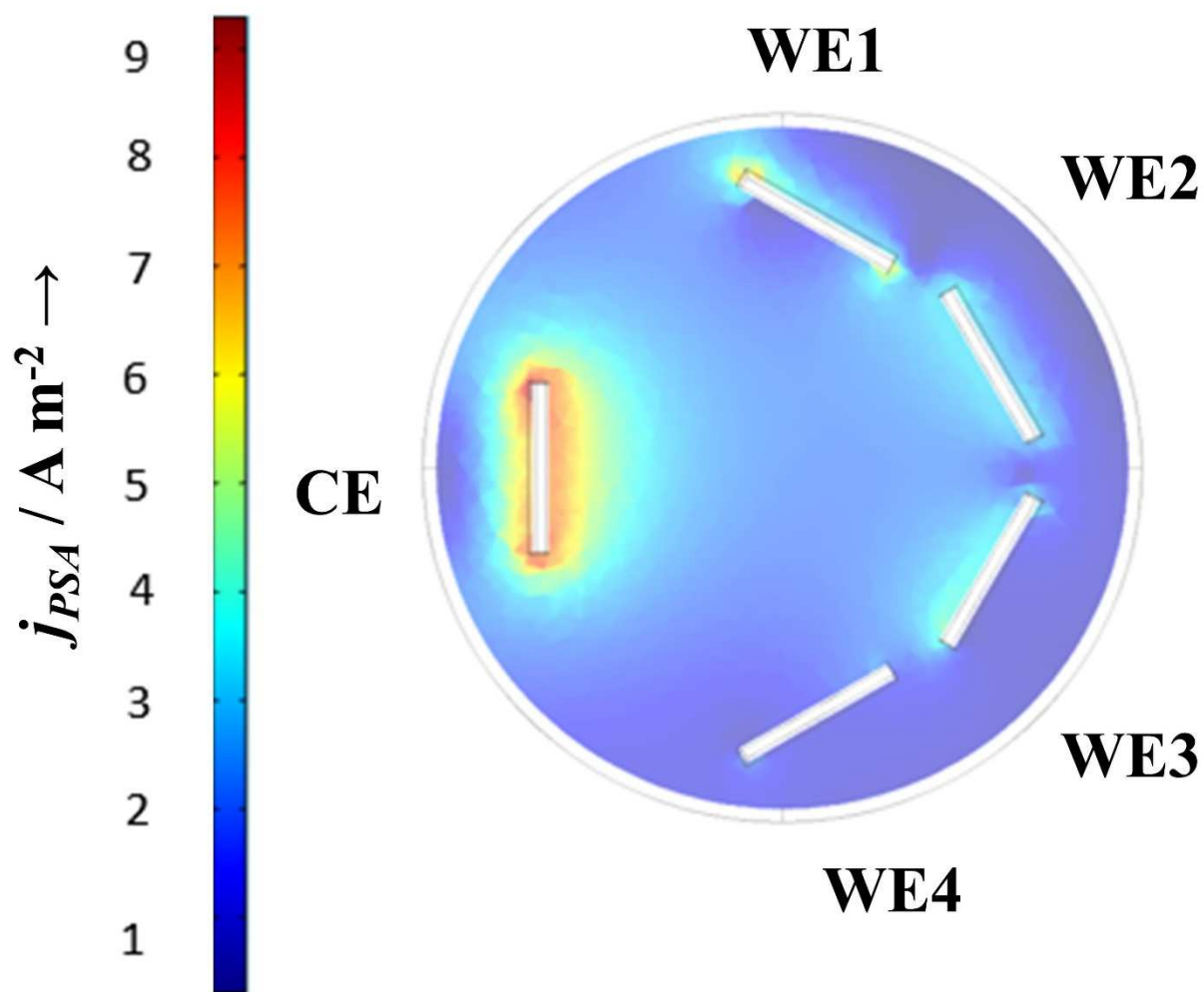


410

411 **Figure 4:**

412

413

414 **Figure 5:**

415

ACCEPTED MANUSCRIPT

Comment citer ce document :

Carmona Martinez, A., Lacroix, R., Trably, E., Da Silva, S., Bernet, N. (Auteur de correspondance) (2018). On the actual anode area that contributes to the current density produced by electroactive biofilms. *Electrochimica Acta*, 259, 395-401. , DOI : 10.1016/j.electacta.2017.10.200

**Highlights**

- Consensus on the anode area contributing to microbial current production is proposed.
- Electrochemistry and microscopy confirm the anode area actively producing current.
- Total immersed area in the electrolyte should be used to calculate current density.
- Sides hidden from cathode shall be electrically insulated to avoid overestimation.

ACCEPTED MANUSCRIPT

Comment citer ce document :

Carmona Martinez, A., Lacroix, R., Trably, E., Da Silva, S., Bernet, N. (Auteur de correspondance) (2018). On the actual anode area that contributes to the current density produced by electroactive biofilms. *Electrochimica Acta*, 259, 395-401. , DOI : 10.1016/j.electacta.2017.10.200